Capillarity

Vol. 16, No. 3, p. 61-76, 2025

Invited review

Competitive adsorption and microscopic wetting properties in CO_2-H_2O-rock systems: A review

Chi Zhang[1], Yan Zhang[2], Yi Su[2], Linyang Zhang[3]*, Xinran Yu[4]

[1]*School of Environmental and Municipal Engineering, Qingdao University of Technology, Qingdao 266520, P. R. China*

[2]*Dongying Economic & Technological Development Zone Administrative Committee, Dongying 257091, P. R. China*

[3]*Key Laboratory of Industrial Fluid Energy Conservation and Pollution Control, Ministry of Education, Qingdao University of Technology, Qingdao 266520, P. R. China*

[4]*College of Pipeline and Civil Engineering, China University of Petroleum (East China), Qingdao 266580, P. R. China*

Keywords:
Microscopic wetting
microscopic adsorption
competitive adsorption
adsorption energy
contact angle

Cited as:
Zhang, C., Zhang, Y., Su, Y., Zhang, L., Yu, X. Competitive adsorption and microscopic wetting properties in CO_2-H_2O-rock systems: A review. Capillarity, 2025, 16(3): 61-76.
https://doi.org/10.46690/capi.2025.09.01

Abstract:
At the microscopic scale, the competitive adsorption of CO_2 and H_2O alters the interfacial characteristics of rock surfaces, thereby inducing significant deviations between the microscopic wetting properties and macroscopic behaviors, a phenomenon critically impacting unconventional hydrocarbon extraction. Consequently, this paper analyzes the interfacial interactions and microscopic adsorption mechanisms of CO_2 and H_2O on rock surfaces at the molecular level and characterizes the properties of their adsorption layers. Building on this foundation, existing models of competitive adsorption and adsorption energy are summarized, revealing how alterations in interfacial properties affect wettability. Furthermore, the influence of surface energy, surface tension, surface roughness, organic content, and pore structure on the contact angle is discussed, along with the applicability and limitations of contact angle theoretical models. Overall, this paper proposes a method to achieve the accurate characterization of microscopic wetting behavior by incorporating correction coefficients (e.g., adsorption energy, surface roughness) into macroscopic models.

1. Introduction

With the growing global energy demand and the ongoing transformation of the energy structure, shale oil has become a critical part of the energy supply and is emerging as a highly promising alternative energy resource. However, shale reservoirs are characterized by huge burial depths, as well as extremely low porosity and permeability (Nie et al., 2023), leading to generally low oil and gas productivity (Yuan et al., 2015; He et al., 2023a; Xu et al., 2023). There is an urgent need to enhance shale oil and gas recovery through engineered fracturing techniques, including gas displacement methods and supercritical fluid displacement processes. Concurrently, the geological storage of CO_2 is a key technology for reducing carbon emissions. Due to the superior adsorption properties of CO_2, organic gases are displaced by CO_2 fracturing. Thus, CO_2 flooding in shale formations constitutes a critical technique for enhanced shale hydrocarbon recovery (Li et al., 2024c). However, microscopic wetting properties govern the distribution and mutual displacement behavior of CO_2 and H_2O, while competitive adsorption between CO_2 and H_2O influences the interfacial properties, pointing to the importance of research on wetting properties in CO_2-H_2O-rock systems.

Yandy Scientific Press

*Corresponding author.
E-mail address: 19898945994@163.com (C. Zhang); zglucy@163.com (Y. Zhang); ting-333@163.com (Y. Su); zhanglinyang@qut.edu.cn (L. Zhang); joyyu94@163.com (X. Yu).

Received May 28, 2025; revised June 22, 2025; accepted July 13, 2025; available online July 16, 2025.

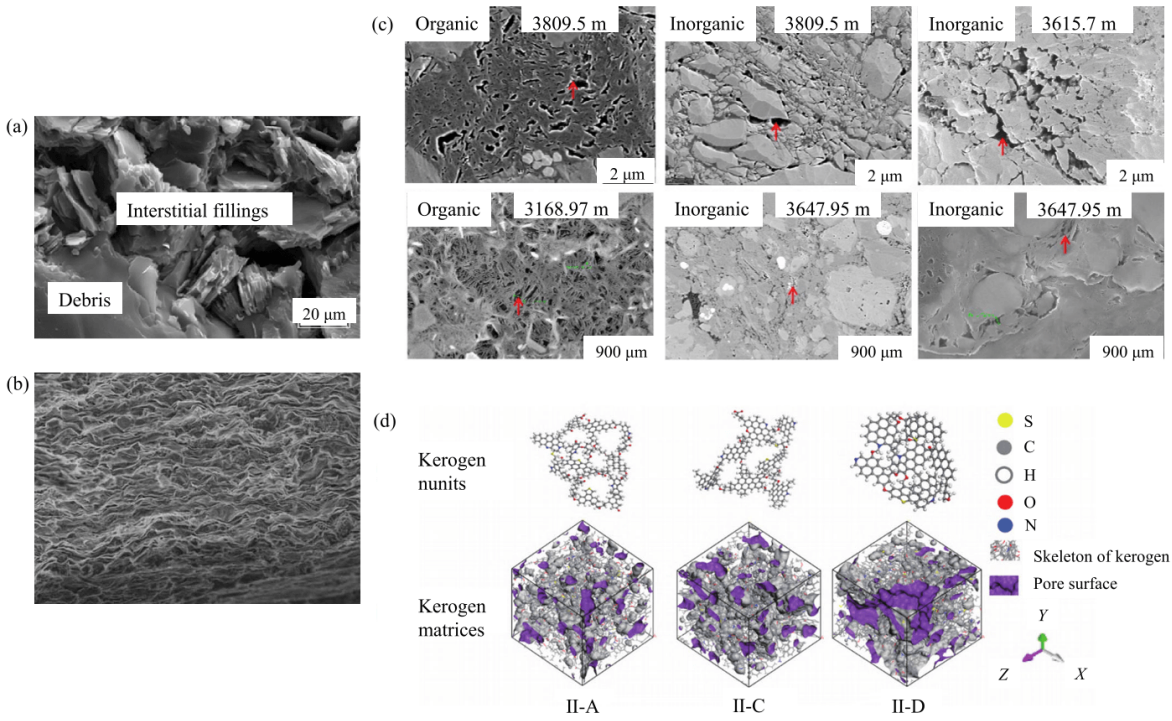

Fig. 1. Inorganic and organic shale pore: (a) Rock micro-computed tomography scanning (Zhang et al., 2025b), (b) Scanning Electron Microscope (SEM) image of montmorillonite (Mouzon et al., 2016), (c) SEM images of nano-organic and inorganic pores in shales from different depths (Ma et al., 2021), and (d) modeling of molecular structural units and condensed matrices of kerogen at different maturity levels (Huang et al., 2019).

Wetting phenomena occur when a liquid adheres to and spreads across a solid surface (Josyula et al., 2024). As a pivotal interfacial characteristic, wetting properties play a critical role in subsurface engineering systems. However, microscopic wetting properties are governed by various molecular-scale forces, including surface tension, van der Waals forces, and electrostatic interactions, which induce marked deviations between microscopic and macroscopic wetting behavior (Deglint et al., 2019; Cao et al., 2024; Qin et al., 2024). Consequently, a fundamental challenge in interfacial science is to elucidate the competitive adsorption mechanisms and adsorption layer properties through interfacial thermodynamics and molecular dynamics to delineate nanoscale wetting mechanisms in CO_2-H_2O-rock systems, enabling the precise characterization of microscopic wetting properties (Jia et al., 2021; Josyula et al., 2024). Recent advances in experimental and molecular simulation techniques have enabled new insights into CO_2-H_2O-rock interfacial wetting properties. Molecular Dynamics Simulation (MD) simulations revealed molecular-scale wetting behavior (Liang et al., 2017), while synchrotron micro-CT was used to probe CO_2-brine interactions in porous media (Lv et al., 2016). Image analysis verified the control mechanisms mediated by wetting properties (Hu et al., 2017). Furthermore, Nabizadeh et al. (2019) identified contact angle as a key multiphase flow parameter via 3D numerical modeling. However, oversimplifying wetting properties through contact angle parameterization overlooks the microscopic complexities (e.g., competitive adsorption and interfacial reconfiguration), causing significant simulation-nanoscale reality discrepancies (Aryana et al., 2023).

This paper summarizes the existing literature to establish a tripartite analytical framework encompassing "molecular adsorption-interfacial reconstruction-pore wetting properties". First, the adsorption mechanisms of CO_2 and H_2O in shale (particularly on montmorillonite and kerogen) are analyzed, and fluid-rock interfacial properties are characterized. Subsequently, the configurations of CO_2 and H_2O adsorption layers are presented, followed by a summary of adsorption energy calculation models. Finally, the factors affecting microscopic wetting properties at three-phase contact interfaces are discussed. This work provides fundamental theoretical references for multiple aspects of interfacial molecular science and subsurface fluid mechanics.

2. Microscopic adsorption

2.1 CO_2/H_2O adsorption behavior in shale

Shale, characterized by clay-rich mineralogy and organic content, features heterogeneous pore systems spanning nanoscale matrix pores to micrometer-scale fractures (Figs. 1(a) and 1(b)) (Jia et al., 2023). These characteristics collectively provide prolific surface sites for gas adsorption (Cai et al., 2024). Shale predominantly consists of inorganic montmorillonite and organic kerogen, whose pore architectures at the nanoscale are different (Fig. 1(c)). As a typical layered silicate clay mineral in shale, montmorillonite exhibits significant adsorption properties by virtue of its microscopic structure.

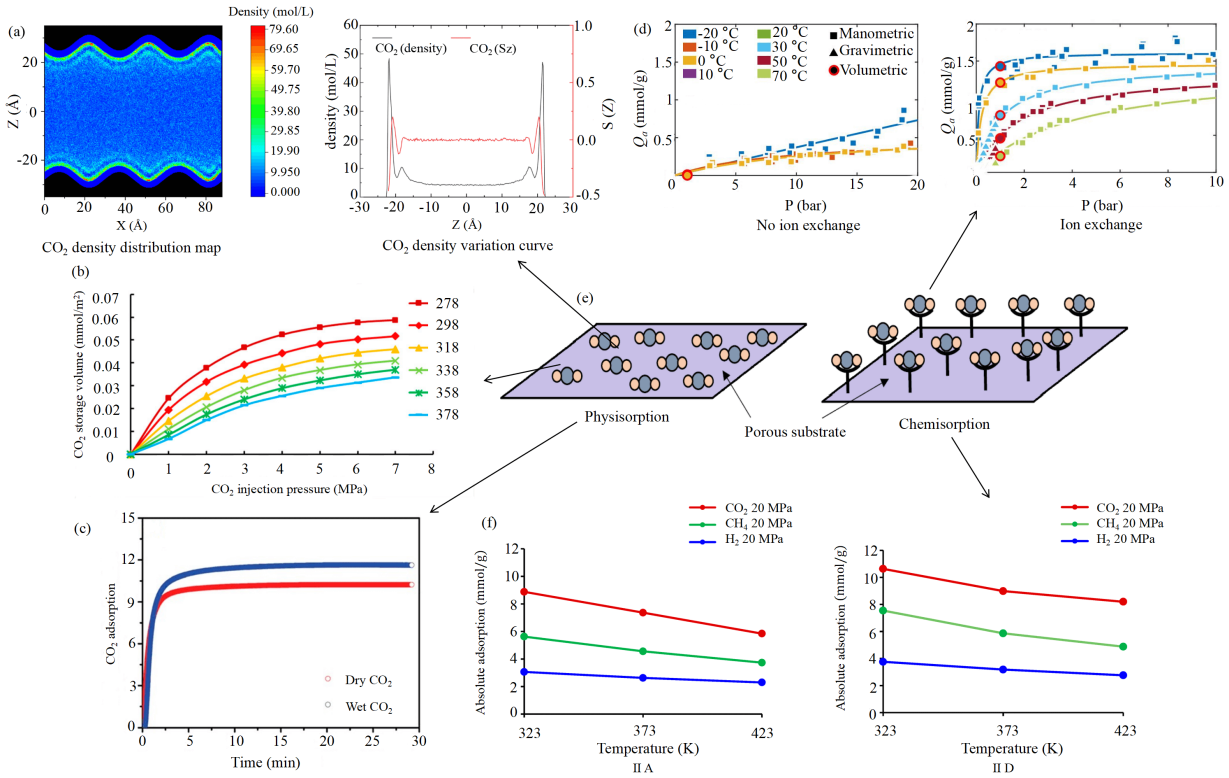

Fig. 2. CO_2 adsorption under varying conditions: (a) CO_2 adsorption in nanopores (Cui et al., 2024), (b) absolute CO_2 adsorption vs. P/T (Hou et al., 2022), (c) CO_2 adsorption vs. humidity (Kolle et al., 2021), (d) adsorption of CO_2 with no ion exchange and ion exchange (Mendel et al., 2021), (e) physisorption and chemisorption (Gunawardene et al., 2022), and (f) CO_2 absolute adsorption vs kerogen maturity (Raza et al., 2022).

Thus, montmorillonite is an essential model for revealing complex microscopic adsorption mechanisms within CO_2-H_2O-rock systems. Montmorillonite exhibits stronger CO_2 adsorption capacity than other shale minerals and kerogens of any maturity, as demonstrated by Materials Studio simulations (Sharma et al., 2015; Wang and Chang, 2024). For organic matter, kerogen exhibits distinct structures at different maturity levels (Fig. 1(d)), with its CO_2 adsorption capacity increasing moderately with higher maturity (Sui et al., 2020).

Montmorillonite adsorbs CO_2/H_2O via dual physical-chemical mechanisms (Nandi and Uyama, 2014; Cabriga et al., 2023). CO_2 exists predominantly in adsorbed state within nanopores (< 10 nm) and as a free phase in larger pores (Fig. 2(a)). Despite elevated temperatures weakening intermolecular forces and electrostatic interactions between CO_2 and montmorillonite, CO_2 adsorption continues to exhibit a minimal yet incremental increase under this condition (Fig. 2(b)) (Du et al., 2020; Hou et al., 2022). Furthermore, Zhang et al. (2025a) proposed that CO_2 adsorption increases proportionally with adsorption time, surface tension, and contact angle. Chemical adsorption predominantly enhances CO_2 adsorption capacity in rocks via interlayer cation exchange (Fig. 2(d)) (Yi et al., 2018; Nowrouzi et al., 2019; Mendel et al., 2021). However, the hydrophilic swelling of montmorillonite enhances its H_2O adsorption capacity. Kerogen adsorption behavior is profoundly governed by its pore architecture and maturity. CO_2 displaces H_2O more effectively in kerogen nanopores, but the adsorption capacity decreases with pore enlargement (Li et al., 2020b). Mature kerogen slightly boosts CO_2 adsorption led by van der Waals forces, whereas immature kerogen demonstrates preferential affinity for H_2O (Fig. 2(f)) (Huang et al., 2018; Lawal et al., 2020; Raza et al., 2022). Additionally, high humidity triggers H_2O clathrate formation, sharply increasing CO_2-H_2O interactions and elevating CO_2 adsorption (Fig. 2(c)) (Kolle et al., 2021).

2.2 Mechanisms of solid-fluid interactions

Solid-fluid interface mechanics essentially reflect the interplay between interfacial energy and intermolecular forces, governed by electrostatic interactions (including hydrogen bonding), surface tension, hydration forces, and hydrophobic effects. Modifying interfacial properties alters electrostatic interactions between H_2O and contact surfaces, inducing hydrophobicity (Li et al., 2007; Monroe et al., 2020; Wang et al., 2021). Hydrophilic liquids exhibit distinct stratification due to hydrogen bonding (Fig. 3(a)), whereas hydrophobic interfaces show minimal stratification (Fig. 3(b)). Moreover, hydrogen bond reorganization enables H_2O to form nanoscale hydration films on contact surfaces (Fig. 3(c)) (Miyazawa et al., 2016). The energy required to remove hydration films determines the hydration forces, whose presence consequently reduces gas adsorption capacity on rock surfaces (Fukuma and

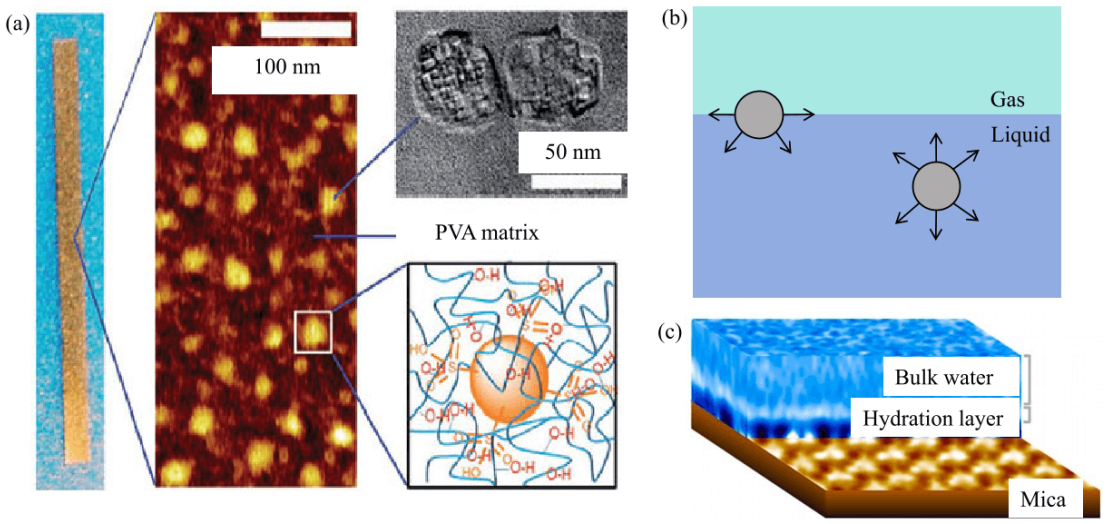

Fig. 3. Fluid-solid interfacial characteristics: (a) Hydrogen bond distribution (Song and Wang, 2020), (b) physical model of surface tension (Van Honschoten et al., 2010), and (c) hydration layers (Fukuma and Garcia, 2018).

Garcia, 2018). Hydrophobic interfaces exhibit long-range attraction far exceeding molecular forces, demonstrating distinct stepwise characteristics due to intervening nanobubbles that modulate hydration forces (Israelachvili and Pashley, 1982; Parker et al., 1994). When the contact angle exceeds 90°, hydration forces begin to attenuate. In addition, surface tension constitutes a fundamental interfacial characteristic. When a liquid contacts a solid, the free energy required to form a stable interface equals the surface tension (Van Honschoten et al., 2010). To this end, adjusting nonpolar group positions effectively modulates surface tension. For weakly polar fluids, minor surface tension variations significantly alter the wetting properties (Hantal et al., 2019; Tian et al., 2020).

3. Competitive adsorption

3.1 CO_2/H_2O competitive adsorption

Investigating CO_2/H_2O competitive adsorption reveals dynamic energy partitioning and the regulation of interfacial wetting properties at the molecular level, where molecular potential energy, electrostatic interactions, charge distribution, and functional group polarities govern the adsorption mechanisms. CO_2/H_2O competitive adsorption is dominated by van der Waals forces, with fundamentally distinct Lennard-Jones potentials and Coulombic contributions (Fig. 4(a)) (Jeong and Kim, 2016). The lower molecular potential energy of CO_2 relative to H_2O induces diminished adsorption capacity on rock surfaces (Fig. 4(c)). The electrostatic interactions (primarily hydrogen bonding) dictate the stabilized adsorption of H_2O. Moreover, H_2O preferentially engages with charged surface groups on rocks through electrostatic forces (Jia et al., 2021; Grekov et al., 2023). Aybar et al. (2025) demonstrated that while water exerts relatively weak electrostatic screening on CO_2-rock interactions, it nevertheless functions as a secondary factor diminishing CO_2 adsorption (Fig. 4(b)). The interplay of van der Waals and electrostatic forces drives adsorbate charge rearrangement at the rock interfaces, governing competitive adsorption, and the emergence of resultant stabilized electric double layers upon reaching adsorption equilibrium (Fig. 4(d)) (Nasralla and Nasr-El-Din, 2014; Wu, 2022). Furthermore, functional group identity and polarity govern competitive adsorption outcomes. For example, surface hydroxylation promotes hydrogen bonding with H_2O (He et al., 2023b; Yeon et al., 2023). The controlled introduction of oxygen-containing functional groups on rock surfaces induces electronic redistribution, thereby enhancing CO_2 adsorption capacity (Fig. 4(e)) (Bai et al., 2015; Yang et al., 2021). The CO_2 adsorption capacity sequence among functional groups is in the descending order of Carboxy > Hydroxy > Carbonyl > Carbon (Fig. 4(f)) (An et al., 2022). Additionally, MD simulations revealed CH_4 enrichment in nanopore concavities, exhibiting CO_2-like distribution. C_2H_6 generally shows greater adsorption capacity than CH_4 due to its enhanced polarity and stronger van der Waals interactions (Liu et al., 2024). However, in nanoscale pores, CH_4 may have higher capacity compared to C_2H_6 (Li et al., 2024a).

3.2 Competitive adsorption models

The Langmuir isothermal adsorption model and the physicochemical mechanism of competitive adsorption are highly compatible. Eqs. (1) and (2) present the Langmuir isothermal adsorption model equations and the three-parameter Langmuir-Freundlich model equations, respectively:

$$V = \frac{V_L p}{P_L + p} \tag{1}$$

$$V = V_L \frac{(K_b p)^n}{1 + (K_b p)^n} \tag{2}$$

where V_L stands for the Langmuir volume; P_L means the Langmuir pressure; p denotes the equilibrium pressure; K_b denotes the binding constant; n is the model parameter.

Scholars have proposed the selectivity coefficient as a critical parameter for characterizing the competitive adsorption characteristics in a multicomponent gas system

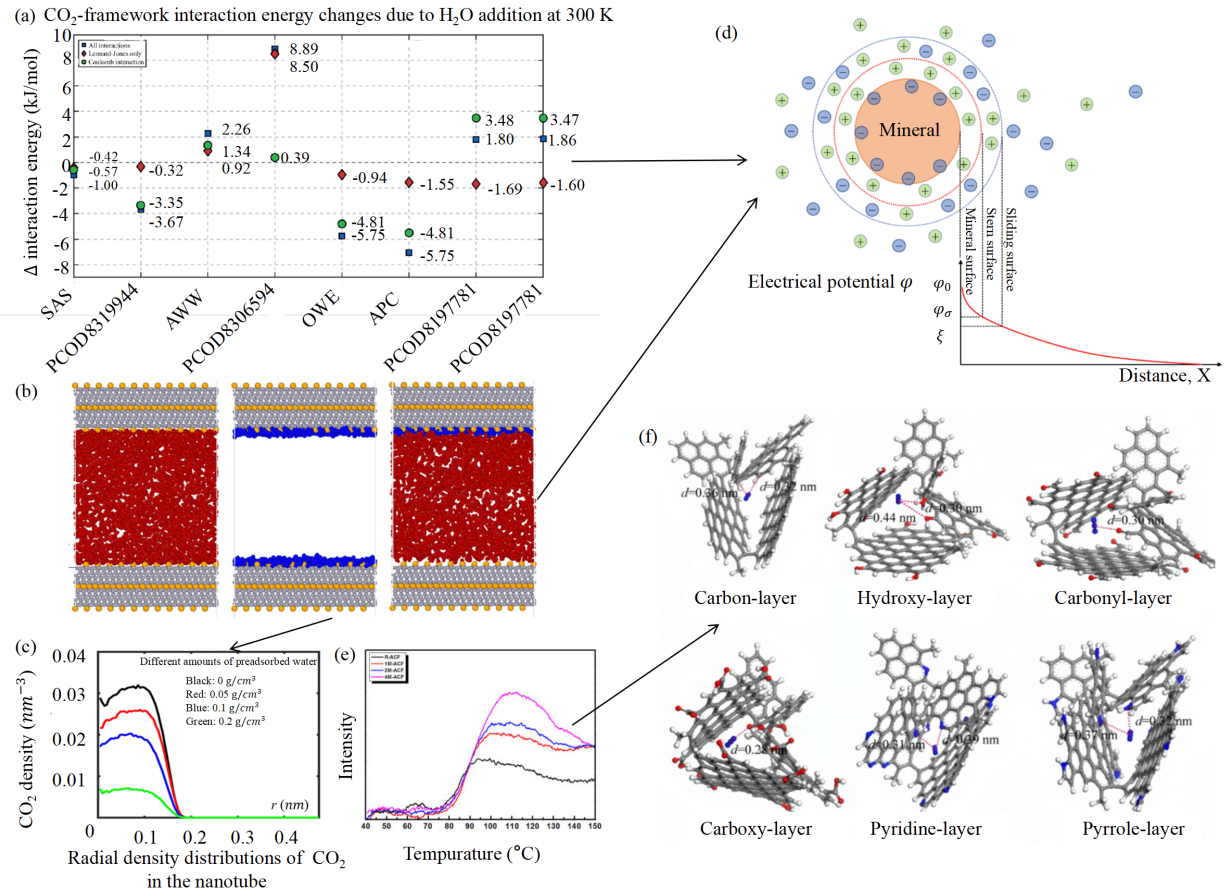

Fig. 4. Competitive adsorption mechanisms between CO_2 and H_2O: (a) CO_2 interaction energy in Sodium Allyl Sulfonate (SAS), PCOD8319944, PCOD8306594, PCOD8197781, PCOD8195213, AWW, OWE, and APC (data from Jeong and Kim (2016)), (b) images of CO_2 and H2O adsorption (red is for CO_2, blue is for H_2O) (Aybar et al., 2025), (c) CO_2 density under different amounts of preabsorbed water (Yang et al., 2020), (d) two-electron layer model (Nasralla and Nasr-El-Din, 2014), (e) adsorption capacity of CO_2: pristine surfaces vs. oxygen-functionalized surfaces at varying temperature (Bai et al., 2015), and (f) optimal geometrical configurations of adsorbed CO_2 at different functional group sites (Fernandez-Alos et al., 2011).

(Ruthven, 1984). Eq. (3) defines the selectivity coefficient for competitive adsorption systems:

$$S_{A/B} = \frac{x_A/x_B}{y_A/y_B} \tag{3}$$

where x_A and x_B respectively represent the gas mole fraction in the adsorption region of A and B; y_A and y_B are respectively the gas mole fraction in the free gas region.

Radial distribution function characterizes microstructural ordering within particulate systems, revealing spatial correlations arising from organized particle aggregation (Kraevsky et al., 2024; Kryuchkov et al., 2024):

$$g_{ab}(r) = \frac{\mathrm{d}N}{4\pi\rho_b r^2 \mathrm{d}r^2} \tag{4}$$

where dN represents the number of b particles within r to $r+\mathrm{d}r$ shells from a atom; ρ_b is the density of particle b.

Mean square displacement quantifies the deviation of a particle's position from its initial reference point over time (Shao et al., 2022). Einstein's formula is currently the predominant computational approach (Didier and Nguyen, 2020; Jawerth et al., 2020):

$$D = \lim_{t\to\infty} \frac{1}{6t} \left\langle |r_i(t) - r_i(0)|^2 \right\rangle \tag{5}$$

where D denotes the diffusion coefficient; $r_i(t)$, $r_i(0)$ are respectively the displacement vector of the molecular center of mass at moments t and 0.

4. Adsorption layer

4.1 Adsorption layer properties

Adsorption layers directly manifest competitive adsorption at the interfaces, which are modulated by pore structure, mineralogy and organic content (Barberi and Spriano, 2021; Sun et al., 2022). Analyzing adsorption layers and adsorption energy thus reveals microscale-macroscale wettability discrepancies, enabling precise adsorption behavior. Firstly, the CO_2 adsorption layer stratifies into contact, inner and transition layers (Fig. 5(a)). Successive adsorption layers form once the preceding layer reaches saturation. Fig. 5(b) depicts the first and second layers of CO_2 on montmorillonite (above) and

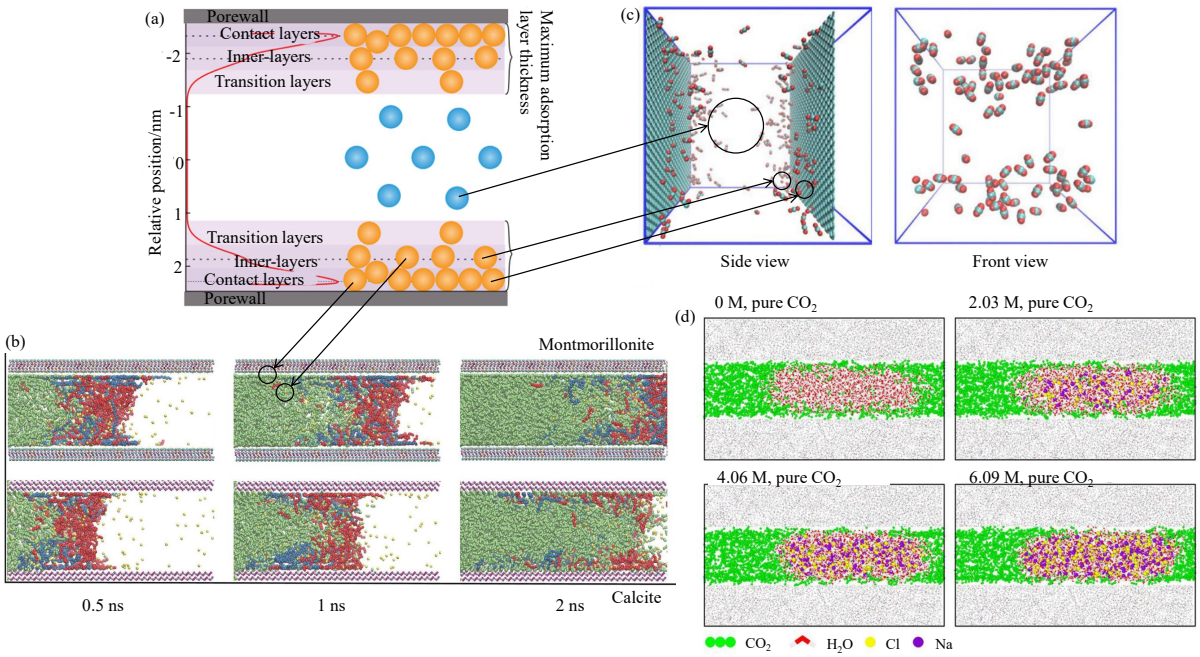

Fig. 5. CO_2 adsorption layers: (a) CO_2 multi-component adsorption layers (Wang et al., 2024), (b) density distributions and adsorption equilibrium configurations of CO_2 (Dong et al., 2023), (c) distribution map of CO_2 molecules (Hu et al., 2024), and (d) equilibrated snapshots of CO_2 and brine in kerogen nanopores with different salinities (Zhou et al., 2020).

calcite (below) surfaces (Wang et al., 2024), while Fig. 5(c) presents the side and top views of CO_2 adsorption layers on the graphene surface (Hu et al., 2024). Both strong and weak adsorption layers coexist under experimental conditions (Xu et al., 2020). Secondly, CO_2 forms discontinuous adsorption layers on slit surfaces, with preferential accumulation in concave regions (Fig. 2(a)) (Lin et al., 2023). Within the CO_2/brine(water)/kerogen system, CO_2 molecules exhibit a tight encapsulation of water/brine clusters, particularly under low-salinity conditions (Fig. 5(d)) (Zhou et al., 2020). Thirdly, increased surface roughness provides more adsorption sites for CO_2 while reducing the peak density of adsorption layers (Tesson and Firoozabadi, 2018; Xu et al., 2024).

Considering the H_2O adsorption layer, it exhibits distinct properties under varying organic matter conditions and pore size constraints. Progressive increases in H_2O mass percentage lead to stable adsorption on mineral surfaces under organic-free conditions (blue parts), whereas organic-bearing matrices (red parts) consistently exhibit self-aggregating molecular clusters of H_2O irrespective of mass percentage elevation (Fig. 6(a)) (Yang et al., 2024). In calcite nanopores, increasing oil mass fractions trigger sequential H_2O adsorption layer transitions. Initially, an aqueous bridging phenomenon emerges, followed by water-oil-water layered structuring (Fig. 6(b)). At critical oil fractions, residual H_2O molecules form adsorption layers on pore surfaces preceding complete displacement by oil (Zhang et al., 2021). H_2O adsorption layers show stratified distribution in small graphene nanopores but not in larger ones (Hu et al., 2024).

4.2 Adsorption energy models

The analysis of adsorption energies provides thermodynamic foundations for investigating the microscopic wetting properties and serves as a critical entry point for revealing the differentials of macro-scale wetting properties. This study systematically compiles adsorption energy theories and their corresponding formulations for distinct applicability categories, as summarized in Table 1. Table 2 presents the calculation formulas for different types of adsorption energy.

The Density Functional Theory (DFT) enables precise microscopic adsorption modeling and pore size distribution (Liao et al., 2022; Yadav et al., 2023). Thermodynamic approaches calculate the adsorption energy, with adsorbed-phase entropy derived from DFT-calculated vibrational frequencies and thermal corrections (Jørgensen et al., 2018; Ferrari and Bennett, 2021). Adsorption selectivity is quantified via adsorbate Gibbs free energy differences:

$$S = \frac{\theta_{CO_2}}{\theta_{H_2O}} = \frac{P_{CO_2}}{P_{H_2O}} \exp\left(-\frac{\Delta G_{ads,CO_2} - \Delta G_{ads,H_2O}}{RT}\right) \quad (6)$$

where S denotes the adsorption selectivity; θ_{CO_2} and θ_{H_2O} are respectively the surface coverages of CO_2 and H_2O; P_{CO_2} and P_{H_2O} are respectively the pressure of CO_2 and H_2O; $\Delta G_{ads,CO_2}$ and $\Delta G_{ads,H_2O}$ are respectively the Gibbs free energy of CO_2 and H_2O.

It is also possible to split the Gibbs free energy into enthalpy and entropy change terms:

Table 1. Theoretical and computational expressions for adsorption energy for different applicable categories.

Adsorption calculation model	Category of application	Formula
Langmuir	Monomolecular layer adsorption theory	$\frac{P}{V(P_0-P)}=\frac{1}{V_mK_L}$
Freundlich	Non-uniform surface or multimolecular layer adsorption	$V=KP^{1/n}$
BET	Multi-molecular layer adsorption theory	$\frac{P}{V(P_0-P)}=\frac{1}{V_mC}\frac{P}{P_0}\frac{C-1}{V_mC}$
Dubinin-Astakhov	Theory of microporous filling based on adsorption potential	$V=V_m\exp\left(-\frac{\varepsilon}{\varepsilon_0}\right)$

Notes: P_0 is the saturation vapot pressure, V is the adsorbed volume, V_m is the monolayer capacity, K_L is the Langmuir constant, K is the freundlich constant, C is the BET constant, ε is the adsorption potential, ε_0 is the characteristic energy.

Table 2. Calculation table for different adsorption energies.

Type	Formula
Density functional theory	$E_{ad}=E_{mg}-E_m-E_g$
DFT's core formula for calculating adsorption energy	$E_{ad}=E_T-E_{TA}-E_{TS}$
Commonly used formulas for theoretical calculation of adsorption energy	$\Delta E_{ads}=E_{AB}-E_A-E_B$
Calculation formula of adsorption energy on coal surface	$E_{BE}=E_{Mm}-E_M-E_m$
Equation for the adsorption energy of and molecules on a model coal surface	$E_{ABE}=E_{MAB}-E_{MB}-E_m$

Notes: E_{ad} is adsorption energy, E_{mg} is total energy of the adsorption system, E_m is the energy of a single gas molecule, E_g is energy of substrate (e.g., graphene). E_T is adsorption of system energy, E_{TA} is the adsorption of system energy, E_{TS} is the substrate energy. ΔE_{ads} is adsorption energy of the adsorbent after adsorption has occurred, E_{AB} is total energy of the entire adsorption system after adsorption occurs, E_A is energy of the adsorbent before adsorption occurs, E_B is energy of the adsorbate before adsorption occurs. E_{BE} is adsorption energy on coal matrix surfaces, E_{Mm} is adsorption energy of a coal surface with gas molecules adsorbed to an equilibrium state, E_M is energy before adsorption on the coal surface, E_m is energy of gas molecules before adsorption. E_{ABE} is adsorption energy of species A during competitive adsorption at coal matrix surface sites, E_{MAB} is adsorption energies of , molecules adsorbed on the coal surface to reach the equilibrium state, E_{MB} is Energy of molecules after adsorption on coal surface.

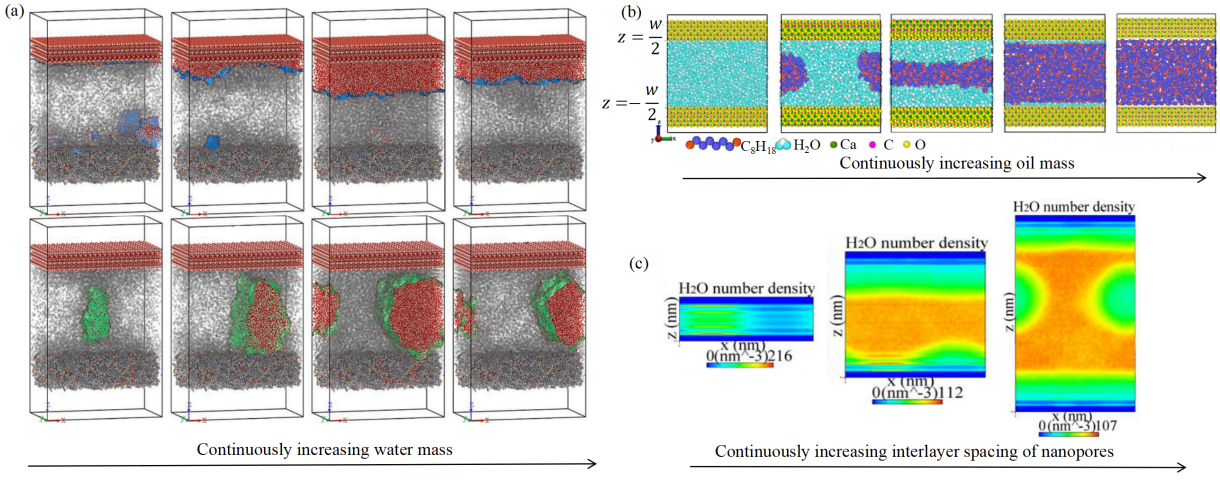

Fig. 6. H_2O adsorption layers: (a) Inorganic (blue) vs. organic (red) conditions (Yang et al., 2024), (b) adsorption layers of H_2O under increasing oil mass percentage in nanopore systems (Zhang et al., 2021), and (c) adsorption layers of H_2O across distinct nanopore systems (Hu et al., 2024).

Table 3. Mathematical expressions for different contact angle models and their applicability.

Model	Mathematical expression	Applicable conditions
Young's equation (Young, 1805)	$\gamma_{sv} - \gamma_{sl} = \gamma_{lv}\cos\theta$	Smooth homogenized surface
Wenzel's wetting model (Wenzel, 1936)	$\cos\theta = r\cos\theta_0$	Rough surfaces (fully wetted)
Cassie-Baxter's wetting model (Cassie and Baxter, 1944)	$\cos\theta_{\text{rough}} = f_{sl}\cos\theta_0 + f_{\text{air}}$	Rough surfaces (gas-liquid coexistence)

Notes: γ_{sv} is surface tension between a gas and a solid, γ_{sl} is surface tension between a gas and a liquid, γ_{lv} is surface tension between a liquid and a solid. r is surface roughness factor, θ_0 is intrinsic contact angle. θ_{rough} is contact angle of a liquid on a rough surface, f_{sl} is fraction of the area of a solid surface covered by liquid, f_{air} is fraction of the area of a solid surface occupied by a gas, $f_{sl} + f_{\text{air}} = 1$.

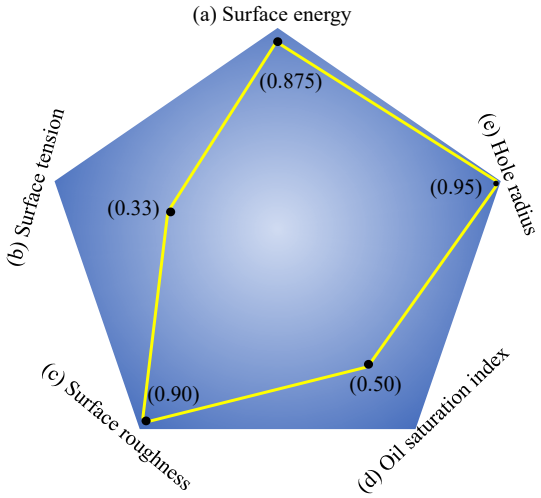

Fig. 7. Factors influencing Contact Angles (CA) (all original data of contributing variables in the radar chart have been normalized to the (0,1) scale, quantitatively reflecting their influence levels from weak to strong): (a) Surface energy ↑, CA ↓, (b) surface tension ↑, CA ↓, (c) surface roughness ↑, the surface transitions from hydrophobic to hydrophilic, CA fistly ↑, then ↓, (d) organic composition↑, CA↑, and (e) hole radius ↓, CA ↓ (the data in (a)-(e) are all sourced from Wang and Zhang (2020), Pan et al. (2018), Youngblood and McCarthy (1999), Wróblewski and Kachel (2023), Afekare et al. (2020)).

$$S = \frac{\theta_{CO_2}}{\theta_{H_2O}} = \frac{P_{CO_2}}{P_{H_2O}} \exp\left(-\frac{\Delta H_{\text{ads},CO_2} - \Delta H_{\text{ads},H_2O}}{RT}\right) \times \exp\left(\frac{\Delta S_{\text{ads},CO_2} - \Delta S_{\text{ads},H_2O}}{R}\right) \quad (7)$$

where $\Delta H_{ads,CO_2}$ and $\Delta H_{ads,H_2O}$ respectively represent the enthalpy change of CO_2 and H_2O; $\Delta S_{ads,CO_2}$ and $\Delta S_{ads,H_2O}$ respectively represent the entropy change of CO_2 and H_2O.

5. Microscopic wetting properties

5.1 Factors influencing contact angles

Contact angles at the nanoscale exhibit marked differences compared to those at the macroscopic scale. They are governed by multiscale factors: Interfacial properties (surface energy and tension), substrate morphology (surface roughness and nanopore size), and organic matter distribution characteristics. Substances exhibiting higher surface energy (e.g., solids rich in oxygen-containing functional groups and aliphatic hydrocarbons) demonstrate smaller contact angles under identical conditions (Fig. 7(a)) (Wang and Zhang, 2020; Cao et al., 2024). However, Young's equation dictates that a liquid with higher surface tension exhibits a larger contact angle on a solid surface, while on the same solid surface it conversely exhibits a smaller contact angle for liquids with lower surface tension (Fig. 7(b)). According to the Wenzel model and Cassie-Baxter equation, an increase in surface roughness reduces the contact angle on hydrophilic surfaces while it increases it on hydrophobic surfaces (Kim et al., 2023; Alhammad et al., 2024; Cao et al., 2024). Higher surface tension correlates with smaller contact angles (Fig. 7(c)) (Youngblood and McCarthy, 1999; Muhammed et al., 2024). Meanwhile, higher surface oil content promotes organic species accumulation, leading to increased contact angles through interfacial modification (Fig. 7(d)) (Mirchi et al., 2022; Wróblewski and Kachel, 2023; Li et al., 2024b). Furthermore, smaller pores correlate with larger contact angles (Fig. 7(e)) (Afekare et al., 2020). Table 3 lists the mathematical expressions for different contact angle models and their applicability.

Li et al. (2024b) modified Young's equation, enhancing its applicability for predicting shale wetting properties:

$$\cos\theta = \Delta\rho\gamma_{cw}I - 1 \quad (8)$$

where θ represents the contact angle; $\Delta\rho$ represents the density difference between gas-liquid; γ_{cw} is the Gas-liquid surface tension; I is the Van der Waals Potential Points.

The Wenzel and Cassie-Baxter models converge into a unified Wenzel-Cassie wetting model describing liquid state transitions on rough surfaces under varying conditions (Bormashenko, 2011; Cao et al., 2024). Zhang et al. (2025c) reformulated the Wenzel model by replacing the conventional roughness factor with a microstructure-dependent roughness ratio γ, defined as a parameter related to the surface microstructure:

$$\cos\theta_{\text{rough}} = \gamma\cos\theta_{\text{smooth}} \quad (9)$$

where θ_{rough} denotes contact angle on rough surface; θ_{smooth} denotes contact angle on smooth surface; γ is roughness factor.

The lattice Boltzmann method quantifies surface microstructure effects on contact angles through droplet simulations (He and Luo, 1997). Li et al. (2020a) extended

this method to thermal systems, while Wang et al. (2023) developed a modified multiphase version for CO_2 huff-n-puff water effects.

5.2 Three-phase wetting properties

Molecular-scale competitive adsorption drives interfacial restructuring that alters the properties of three-phase contact line, fundamentally governing microscopic wetting property changes. Thus, these mechanisms are controlled by rock surface structures and molecular interactions. CO_2-H_2O-rock interactions increase hydrophilic group density, enhancing surface hydrophilicity (Zheng et al., 2024). Increased pore water saturation reduces pore volume via complete water occupancy, altering the wetting properties at the rock surface (Selem et al., 2022); the presence of organic matter, although sometimes limited, also exhibits a measurable effect on shale wetting properties (Deng et al., 2025). Molecular simulations of water-montmorillonite interactions reveal precursor films at advancing fronts, exhibiting rapid propagation, expanding diffusion radii, and decreasing contact angles during constant-velocity advancement (Kashkooli et al., 2022; Yan et al., 2024). The microscopic wetting properties of rock constitute a critical factor dictating rock-fluid behavior and macroscopic properties. Within porous media, wetting properties directly govern fluid phase distribution, the resultant force distributions, and relative permeability (Xu et al., 2017; Khan et al., 2024). Alterations in pore-scale wetting properties can induce the remobilization of non-wetting phases under elevated capillary pressures (Nemer et al., 2021). Furthermore, ionic reactions between CO_2 and minerals significantly alter rock morphology, porosity and permeability. Differences in the capillary-driven wetting properties between inorganic/organic shale pores fundamentally influence fluid dynamics, particularly methane-water relative permeability and transport (Zhang et al., 2023). Alterations in the wetting properties have cascading effects across molecular-to-macroscopic scales.

6. Discussion

6.1 Microscopic competitive adsorption

The competitive adsorption of H_2O and H_2O is intricately linked to molecular properties, interfacial ion exchange, van der Waals and electrostatic interactions, Gibbs free energy, and environmental factors. The smaller size of CO_2 enhances diffusion, while its zero-dipole moment and uniform charge distribution lead to weaker adsorption than highly polar H_2O. H_2O displaces CO_2 near Na^+ sites, relocating CO_2 to pore edges and strengthening H_2O-Na^+ bonds (Fig. 8(a)) (Purdue and Qiao, 2018). Increased H_2O adsorption forms H-bonded hydration networks (Joos et al., 2013), and that Na^+ is fully solvated by H_2O (Rao and Leng, 2016). Extensive water condensation forms robust H-bond networks, overwhelming CO_2-adsorbent van der Waals forces and drastically reducing CO_2 capacity. However, strategic surface functionalization can promote carbon participation in hydrogen bonding, competitively disrupting aqueous H-bond networks (Karas et al., 2020). Under thermodynamic regulation, competitive adsorption is governed by the Gibbs free energy, jointly driven by enthalpy changes and entropy contributions (Fig. 8(b)). More negative ΔG_3 values enhance CO_2 adsorption affinity (Fig. 8(c)) (Zhao et al., 2021). Elevated temperatures favor the adsorption of CO_2 over H_2O, while lower temperatures induce H_2O clustering that blocks pores and impedes CO_2 diffusion (Fan et al., 2025). Dry conditions show humidity-independent gas-water interactions, whereas high humidity forms water cages entrapping gas molecules, reducing CO_2 displacement. (Fig. 8(d)) (Shen and Worek, 1994; Kolle et al., 2021; Fu and Davis, 2022). Additionally, hydrophobic surfaces exhibit pressure-dependent contact angle increases, whereas hydrophilic surfaces maintain static wetting properties, indicating that hydrophobic interfaces exert a stronger influence on competitive adsorption (Liang et al., 2017).

6.2 Competitive adsorption alters interfacial properties

CO_2/H_2O competitive adsorption critically modifies the adsorption layer properties by modulating van der Waals forces and electrostatic interactions (e.g., hydrogen bonding), thereby altering interfacial charge density. This process changes adsorption enthalpy/entropy, controlling interfacial adsorption energy. Notably, despite the weaker polarity of CO_2, enhancing long-range electrostatic interactions between CO_2 and H_2O significantly increases the compactness of CO_2 adsorption layer (Jeong and Kim, 2016). Competitive adsorption also changes the interfacial charge distribution. From Eqs. (6) and (7), it can be concluded that the competitive adsorption of CO_2 and H_2O changes the magnitude of adsorption energy (Jørgensen et al., 2018). According to classical electrostatics, the outward local induced stress on this surface is $\varepsilon E^2/2$, and it is a dielectric constant. On the basis of the Young-Laplace equation ($\Delta p = \gamma\kappa$), it is obtained by the combination of these two forces (Van Honschoten et al., 2010):

$$\Delta p = \gamma\kappa - \frac{1}{2}\varepsilon E^2 \tag{10}$$

where Δp denotes pressure difference; γ denotes surface tension; κ denotes curvature of interface; ε denotes permittivity; E denotes electric field strength.

Competitive adsorption between CO_2 and H_2O critically modulates the wetting properties at the three-phase interface (Ballah et al., 2016). Studies have revealed that increasing CO_2 pressure reduces the water-wetting properties (Fauziah et al., 2018), particularly near the supercritical CO_2 threshold of 7.38 MPa (Fang et al., 2016; Yan et al., 2024). The static contact angles on quartz surfaces rise with CO_2 pressure, peaking at 7.2 MPa, while montmorillonite systems exhibit complete wetting under asymmetric Na^+ distribution (Hubao et al., 2023). Supercritical CO_2 further drives the reversal of wetting properties, shifting rock surfaces toward hydrophobicity (Iglauer et al., 2015; Hu et al., 2017), though quartz-dominated reservoirs retain hydrophilicity (Pan et al., 2020; Fatah et al., 2021).

6.3 Contact angle model constraints

Two wetting states can arise: Partial and complete wetting (Fig. 9(a)) (Widom, 2004). However, significant discrepancies

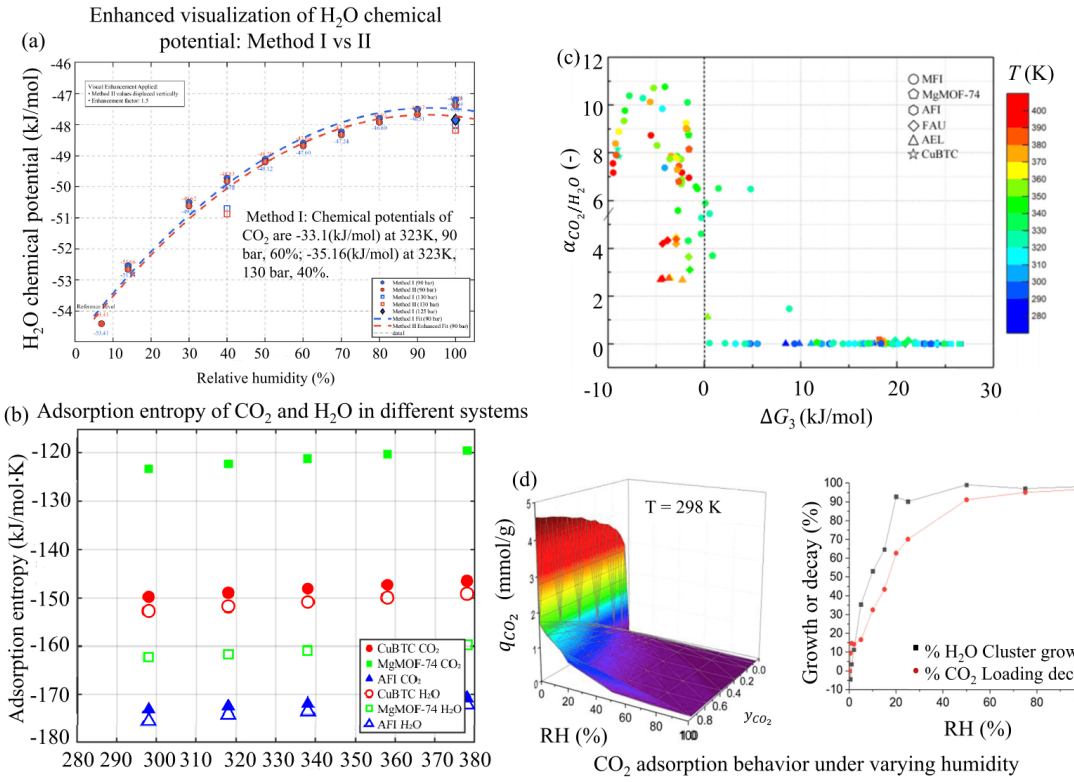

Fig. 8. Factors governing competitive adsorption: (a) Chemical potentials of H_2O and CO_2 (data from Rao and Leng (2016)), (b) Gibbs free energies of CO_2 and H_2O (data from Chaconas et al. (2021)), (c) correlation between Gibbs free energy and selectivity coefficient (Zhao, 2022) and (d) CO_2 adsorption behavior under varying humidity (Purdue and Qiao, 2018).

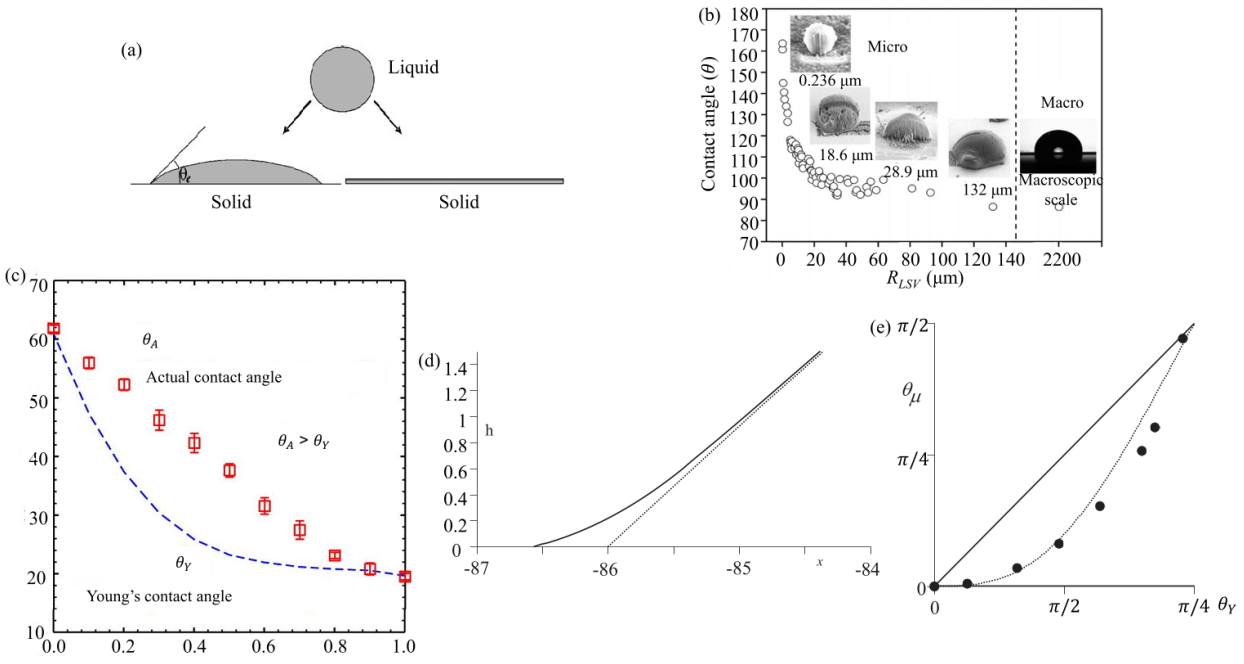

Fig. 9. Limitations of contact angle: (a) Partial wetting (left) and complete wetting (right) (Van Honschoten et al., 2010), (b) contact angles of droplets at different sizes (Park et al., 2015), (c) deviation between the predicted values of contact angle by Young's equation and the actual values (Cheng et al., 2020), (d) microscopic planner surface of a contact line with slope changes (Snoeijer and Andreotti, 2008), and (e) relationship between macroscopic contact angle θ_∞ and microscopic contact angle θ_μ.

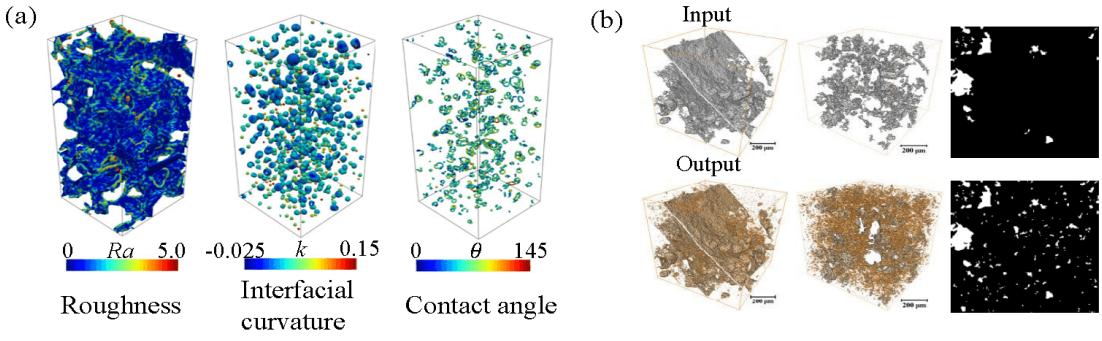

Fig. 10. (a) 3D visualization of the spatial distribution of roughness, interfacial curvature and contact angle (Alzahrani et al., 2024), and (b) multi-scale digital rock (Yang et al., 2022).

exist between nanoscale and macroscopic contact angles (Fig. 9(b)), leading to pronounced deviations between conventional wetting equations and actual computational data (Fig. 9(c)). At macroscopic scales, Young's equation rigorously characterizes the equilibrium state of liquid under partial wetting conditions in a homogeneous solid. However, surface tension cannot fully define interfacial equilibrium; thus, microscopic-scale analysis is essential to resolve force balance. In a vacuum, the van der Waals forces of two neutral molecules (A and B) are expressed as (Van Honschoten et al., 2010):

$$V_{AB} = -k\alpha_A\alpha_B\frac{1}{r^6} \tag{11}$$

where α_A and α_B respectively denote the electrode polarizations of molecules A and B; k is a constant term independent of the nature of A and B; r is the distance between the centers of A and B molecules.

Fig. 9(d) shows the numerical results calculated by Eqs. (10) and (11). The two lines represent changes in the macroscopic contact angle to microscopic contact angle in the vicinity of contact line, and this relationship is approximated by the following expression (Van Honschoten et al., 2010):

$$\theta_\mu \approx \frac{1}{2}\theta_\infty(2-\cos\theta_\infty-\cos^2\theta_\infty) \tag{12}$$

where θ_μ and θ_∞ respectively denote the microscopic and macroscopic contact angle.

Fig. 9(e) visualizes the relationship between macroscopic contact angle and microscopic contact angle derived from the numerical calculations results. This demonstrates that contact angles are collectively determined by microscopic interactions. In the figure, the black dots represent the numerical results of the explicit evaluation of energy generalization, the dashed line is the interpolation based on the local approximation of Eq. (12), and the solid line: θ_∞ = comparative analysis (Snoeijer and Andreotti, 2008).

Furthermore, molecular simulations exhibit deviations from the experimental data. Such cross-scale discrepancies necessitate refinement via in situ characterization techniques (Chen et al., 2024). Illustratively, Alzahrani et al. (2024) developed Micro-Graph-Nets (graph-neural-network framework) to automate microscopic wetting characterization in porous media, simulating surface roughness, interfacial curvature, and spatial contact angles using 3D visualization (Fig. 10(a)). Song et al. (2024) addressed the limitations of existing pore models through multiscale digital rock reconstruction (Fig. 10(b)), revealing nanopore-scale fluid transport. Crucially, conventional macroscopic contact angle models rely solely on temperature and pressure, whereas microscopic wettability is dominated by adsorption phenomena, with adsorption energy as the key interaction parameter. Thus, integrating adsorption energy into a unified temperature-pressure-adsorption energy framework overcomes traditional model limitations, significantly enhancing accuracy for CO_2 displacement and geological sequestration.

7. Conclusions and outlook

7.1 Conclusions

1) The microscopic wetting properties in a CO_2-H_2O-rock system are controlled by physical adsorption, pore structure and surface chemistry. Montmorillonite interlayer cations boost CO_2 adsorption via quadrupole interactions, whereas kerogen maturation regulates adsorption through van der Waals and electrostatic forces.
2) H_2O enhances adsorption via hydrogen bonding, while CO_2 relies on Coulombic/quadrupolar interactions, and their competition causes nonlinear contact angle variations. Multiscale analysis progresses from adsorption selectivity to Gibbs energy differentials and interfacial charge density, revealing competitive adsorption mechanisms.
3) Adsorption layer thickness/distribution controls surface tension and contact angles. CO_2 adsorption dominates in micro/nanopores, while free CO_2 prevails macroscopically, requiring cross-scale adsorption-free equilibrium regulation for the prediction of wetting properties.
4) Microscopic surface energy controls contact angles in two aspects: Higher energy reduces θ, while organic-rich rocks increase via hydrophobicity. These interfacial complexities govern competitive adsorption and contact angle scaling.
5) Young's equation deviates in micro/nanopores due to MD-microfluidic scale disparities. Adsorption energy corrections bridge models of molecular-macroscopic wetting properties, resolving Young's limitations and enabling multiscale "adsorption energy-distribution-contact angle"

quantification.

7.2 Outlook

The analysis of CO_2-H_2O-rock microscopic wetting properties and adsorption mechanisms reveals critical knowledge gaps between microscopic and macroscopic scale behaviors, guiding future research priorities in three ways:

1) The proportional impacts of van der Waals/electrostatic forces on competitive adsorption across mineral surfaces remain unquantified, as do the effects of adsorption layers on surface tension.
2) The coupled effects of temperature-pressure, mineral-fluid chemistry and pore structure on microscopic wetting properties are still unclear, necessitating the identification of dominant controlling mechanisms.
3) The microscopic interfacial parameters cannot be characterized by macroscopic theoretical models, and there is a lack of a cross-scale theoretical framework. Existing predictions exhibit deviations from experimental data obtained via microfluidics and AFM of several orders of magnitude, highlighting the need for unified multiscale models.

Acknowledgements

This research was funded by Natural Science Foundation of Shandong Province (Nos. ZR2022QB046 and ZR2022QE038); the National Natural Science Foundation of China (Nos. 52204039 and 52304059); and the Key R&D Program (Competitive Innovation Platform) of Shandong Province (No. 2022CXPT051).

Conflict of interest

The authors declare no competing interest.

References

Afekare, D., Garno, J. C., Rao, D. Insights into nanoscale wettability effects of low salinity and nanofluid enhanced oil recovery techniques. Energies, 2020, 13(17): 4443.

Alhammad, F., Ali, M., Yekeen, N., et al. The influence of methyl orange on the CO_2-brine wettability of organic-acid-aged calcite samples: Implications for CO_2 geo-storage. Advances in Geo-Energy Research, 2024, 12(2): 102-112.

Alzahrani, M. K., Shapoval, A., Chen, Z., et al. Micro-graphnets: Automated characterization of the micro-scale wettability of porous media using graph neural networks. Capillarity, 2024, 12(3): 57-71.

An, X., Zhao, K., Zhang, W., et al. Tailoring the pore structure modified with functional groups for superior CO_2 adsorption capacity and the selectivity of separation. Fuel, 2022, 309: 122175.

Aryana, S., Kovscek, A., Prodanović, M., et al. The international symposium on wettability and porous media-past, present, and the future. Paper IPJ 240824-3 Presented at 15th International Symposium on Wettability and Porous Media, Laramie, Wyoming, 23-25 October, 2023.

Aybar, M., Zhang, H., Qiao, R., et al. Molecular structure and thermodynamics of CO_2 and water adsorption on mica. The Journal of Physical Chemistry B, 2025, 129(18): 4558-4568.

Bai, B. C., Kim, E. A., Lee, C. W., et al. Effects of surface chemical properties of activated carbon fibers modified by liquid oxidation for CO_2 adsorption. Applied Surface Science, 2015, 353: 158-164.

Ballah, J., Chamerois, M., Durand-Vidal, S., et al. Effect of chemical and geometrical parameters influencing the wettability of smectite clay films. Colloids and Surfaces A: Physicochemical and Engineering Aspects, 2016, 511: 255-263.

Barberi, J., Spriano, S. Titanium and protein adsorption: An overview of mechanisms and effects of surface features. Materials, 2021, 14(7): 1590.

Bormashenko, E. General equation describing wetting of rough surfaces. Journal of Colloid and Interface Science, 2011, 360(1): 317-319.

Cabriga, C. K. C., Clarete, K. V. B., Zhang, J. A. T., et al. Evaluation of biochar derived from the slow pyrolysis of rice straw as a potential adsorbent for carbon dioxide. Biomass Conversion and Biorefinery, 2023, 13(9): 7887-7894.

Cai, J., Jiao, X., Wang, H., et al. Multiphase fluid-rock interactions and flow behaviors in shale nanopores: A comprehensive review. Earth-Science Reviews, 2024, 257: 104884.

Cao, X., Ma, Y., Cao, H., et al. Molecular dynamics simulation study on the wetting characteristics of carbon dioxide droplets on smooth and rough surfaces. Journal of Molecular Liquids, 2024, 403: 124835.

Cassie, A., Baxter, S. Wettability of porous surfaces. Transactions of the Faraday Society, 1944, 40: 546-551.

Chaconas, D., Pichardo, P., Manousiouthakis, I. V., et al. Equilibrium analysis of CH_4, CO, CO_2, H_2O, H_2, C mixtures in C-H-O atom space using gibbs free energy global minimization. American Institute of Chemical Engineers Journal, 2021, 67(1): e17052.

Chen, Y., Seyyedi, M., Clennell, B. Petrophysical recipe for in-situ CO_2 mineralization in basalt rocks. Advances in Geo-Energy Research, 2024, 11(2): 152-160.

Cheng, Y., Chu, K., Tsao, H. K., et al. Size-dependent behavior and failure of young's equation for wetting of two-component nanodroplets. Journal of Colloid and Interface Science, 2020, 578: 69-76.

Cui, J., Bao, J., Ning, S., et al. Molecular simulation of the impact of surface roughness on carbon dioxide adsorption in organic-rich shales. Unconventional Resources, 2024, 4: 100071.

Deglint, H., Clarkson, C., Ghanizadeh, A., et al. Comparison of micro-and macro-wettability measurements and evaluation of micro-scale imbibition rates for unconventional reservoirs: Implications for modeling multi-phase flow

at the micro-scale. Journal of Natural Gas Science and Engineering, 2019, 62: 38-67.

Deng, X., Kamal, M. S., Hussain, S. M. S., et al. Impact of organic acid molecular length and structure on rock oil-wetting rapidity and stability. Journal of Molecular Structure, 2025, 1321: 140009.

Didier, G., Nguyen, H. Asymptotic analysis of the mean squared displacement under fractional memory kernels. Society for Industrial and Applied Mathematics Journal on Mathematical Analysis, 2020, 52(4): 3818-3842.

Dong, X., Xu, W., Liu, H., et al. Molecular insight into the oil displacement mechanism of CO_2 flooding in the nanopores of shale oil reservoir. Petroleum Science, 2023, 20(6): 3516-3529.

Du, X., Guang, W., Cheng, Y., et al. Thermodynamics analysis of the adsorption of CH_4 and CO_2 on montmorillonite. Applied Clay Science, 2020, 192: 105631.

Fan, W., Xin, Q., Dai, Y., et al. Competitive transport and adsorption of CO_2/H_2O in the graphene nano-slit pore: A molecular dynamics simulation study. Separation and Purification Technology, 2025, 353: 128394.

Fang, T., Shi, J., Sun, X., et al. Supercritical CO_2 selective extraction inducing wettability alteration of oil reservoir. The Journal of Supercritical Fluids, 2016, 113: 10-15.

Fatah, A., Bennour, Z., Mahmud, H. B., et al. Surface wettability alteration of shales exposed to CO_2: Implication for long-term integrity of geological storage sites. International Journal of Greenhouse Gas Control, 2021, 110: 103426.

Fauziah, C. A., Al-Yaseri, A. Z., Beloborodov, R., et al. Carbon dioxide/brine, nitrogen/brine, and oil/brine wettability of montmorillonite, illite, and kaolinite at elevated pressure and temperature. Energy & Fuels, 2018, 33(1): 441-448.

Fernandez-Alos, V., Watson, J. K., vander Wal, R., et al. Soot and char molecular representations generated directly from HRTEM lattice fringe images using Fringe3D. Combustion and Flame, 2011, 158(9): 1807-1813.

Ferrari, B. C., Bennett, C. J. A computational investigation of the equilibrium geometries, energetics, vibrational frequencies, infrared intensities and Raman activities of C_2Oy ($y = 3,4$) species. Molecular Physics, 2021, 119(6): e1837404.

Fu, D., Davis, M. E. Carbon dioxide capture with zeotype materials. Chemical Society Reviews, 2022, 51(22): 9340-9370.

Fukuma, T., Garcia, R. Atomic-and molecular-resolution mapping of solid-liquid interfaces by 3D atomic force microscopy. American Chemical Society Nano, 2018, 12(12): 11785-11797.

Grekov, D. I., Robinet, J. C., Grambow, B. Adsorption of methane and carbon dioxide by water-saturated clay minerals and clay rocks. Applied Clay Science, 2023, 232: 106806.

Gunawardene, O. H., Gunathilake, C. A., Vikrant, K., et al. Carbon dioxide capture through physical and chemical adsorption using porous carbon materials: A review. Atmosphere, 2022, 13(3): 397.

Hantal, G. R., Sega, M., Horvai, G., et al. Contribution of different molecules and moieties to the surface tension in aqueous surfactant solutions. The Journal of Physical Chemistry C, 2019, 123(27): 16660-16670.

He, X., Luo, L. A priori derivation of the lattice Boltzmann equation. Physical Review E, 1997, 55(6): R6333.

He, Y., Wang, J., Huang, X., et al. Investigation of low water recovery based on gas-water two-phase low-velocity Non-Darcy flow model for hydraulically fractured horizontal wells in shale. Petroleum, 2023a, 9(3): 364-372.

He, M., Zhao, H., Yang, X., et al. Reconsideration about the competitive adsorption of H_2O and CO_2 on carbon surfaces: The influence of oxygen functional groups. Journal of Environmental Chemical Engineering, 2023b, 11(6): 111288.

Hou, D., Gong, F., Tang, H., et al. Molecule simulation of CH_4/CO_2 competitive adsorption and CO_2 storage in shale montmorillonite. Atmosphere, 2022, 13(10): 1565.

Hu, M., Gao, W., Zhang, L., et al. Simulation study on diffusion and local structure of CH_4, CO_2, SO_2, and H_2O mixtures into double-layers graphene. The Journal of Physical Chemistry B, 2024, 128(46): 11402-11416.

Hu, R., Wan, J., Kim, Y., et al. Wettability impact on supercritical CO_2 capillary trapping: Pore-scale visualization and quantification. Water Resources Research, 2017, 53(8): 6377-6394.

Huang, L., Ning, Z., Wang, Q., et al. Molecular simulation of adsorption behaviors of methane, carbon dioxide and their mixtures on kerogen: Effect of kerogen maturity and moisture content. Fuel, 2018, 211: 159-172.

Huang, L., Ning, Z., Wang, Q., et al. Molecular insights into kerogen deformation induced by CO_2/CH_4 sorption: Effect of maturity and moisture. Energy & Fuels, 2019, 33(6): 4792-4805.

Hubao, A., Yang, Z., Hu, R., et al. Molecular origin of wetting characteristics on mineral surfaces. Langmuir: the American Chemical Society Journal of Surfaces and Colloids, 2023, 39(8): 2932-2942.

Iglauer, S., Pentland, C., Busch, A. CO_2 wettability of seal and reservoir rocks and the implications for carbon geosequestration. Water Resources Research, 2015, 51(1): 729-774.

Israelachvili, J., Pashley, R. The hydrophobic interaction is long range, decaying exponentially with distance. Nature, 1982, 300(5890): 341-342.

Jawerth, L., Fischer-Friedrich, E., Saha, S., et al. Protein condensates as aging maxwell fluids. Science, 2020, 370(6522): 1317-1323.

Jeong, W., Kim, J. Understanding the mechanisms of CO_2 adsorption enhancement in pure silica zeolites under humid conditions. The Journal of Physical Chemistry C, 2016, 120(41): 23500-23510.

Jia, Z., Ning, Z., Gao, X., et al. Experimental investigation on molecular-scale mechanism of wettability alteration induced by supercritical carbon dioxide-water-rock reaction. Journal of Petroleum Science and Engineering, 2021, 205: 108798.

Jia, C., Xiao, B., You, L., et al. Experimental study of

water imbibition characteristics of the lacustrine shale in Sichuan Basin. Petroleum, 2023, 9(4): 572-578.

Joos, L., Swisher, J. A., Smit, B. Molecular simulation study of the competitive adsorption of H_2O and CO_2 in zeolite 13X. Langmuir, 2013, 29(51): 15936-15942.

Jørgensen, M., Chen, L., Gronbeck, H. Monte carlo potential energy sampling for molecular entropy in zeolites. The Journal of Physical Chemistry C, 2018, 122(35): 20351-20357.

Josyula, T., Kumar Malla, L., Thomas, T. M., et al. Fundamentals and applications of surface wetting. Langmuir, 2024, 40(16): 8293-8326.

Karas, L. J., Wu, C. H., Das, R., et al. Hydrogen bond design principles. Wiley Interdisciplinary Reviews: Computational Molecular Science, 2020, 10(6): e1477.

Kashkooli, S. B., Gandomkar, A., Riazi, M., et al. Coupled optimization of carbon dioxide sequestration and CO_2 enhanced oil recovery. Journal of Petroleum Science and Engineering, 2022, 208: 109257.

Khan, M. J., Mahmood, S. M., Alakbari, F. S., et al. Rock wettability and its implication for caprock integrity in CO_2-brine systems: A comprehensive review. Energy & Fuels, 2024, 38(21): 19966-19991.

Kim, K., Kundzicz, P. M., Makhnenko, R. Y. Effect of CO_2 injection on the multiphase flow properties of reservoir rock. Transport in Porous Media, 2023, 147(2): 429-461.

Kolle, J. M., Fayaz, M., Sayari, A. Understanding the effect of water on CO_2 adsorption. Chemical Reviews, 2021, 121(13): 7280-7345.

Kraevsky, S. V., Valueva, A. A., Ershova, M. O., et al. Using the radial distribution function to analyze atomic force microscopy images of colloidal systems. International Journal of Molecular Sciences, 2024, 26(1): 210.

Kryuchkov, N. P., Nasyrov, A. D., Denisenko, I. R., et al. Interpolating the radial distribution function in a two-dimensional fluid across a wide temperature range. The Journal of Chemical Physics, 2024, 161: 094505.

Lawal, L. O., Olayiwola, T., Abdel-Azeim, S., et al. Molecular simulation of kerogen-water interaction: Theoretical insights into maturity. Journal of Molecular Liquids, 2020, 299: 112224.

Li, W., Cao, J., Liang, Y., et al. Molecular simulation of methane/ethane mixture adsorption behavior in shale nanopore systems with micropores and mesopores. Fuel, 2024a, 358: 130294.

Li, Y., Chen, Y., Zhao, J., et al. Interaction mechanism between supercritical carbon dioxide and shale. Oil & Gas Geology, 2024b, 45(4): 1180-1194. (in Chinese)

Li, L., Lu, J., Fang, H., et al. Lattice Boltzmann method for fluid-thermal systems: Status, hotspots, trends and outlook. IEEE Access, 2020a, 8: 27649-27675.

Li, X., Reinhoudt, D., Crego-Calama, M. What do we need for a superhydrophobic surface? A review on the recent progress in the preparation of superhydrophobic surfaces. Chemical Society Reviews, 2007, 36(8): 1350-1368.

Li, W., Zhang, M., Nan, Y., et al. Molecular dynamics study on CO_2 storage in water-filled kerogen nanopores in shale reservoirs: Effects of kerogen maturity and pore size. Langmuir, 2020b, 37(1): 542-552.

Li, L., Zhang, D., Su, Y., et al. Microfluidic insights into CO_2 sequestration and enhanced oil recovery in laminated shale reservoirs: Post-fracturing interface dynamics and micro-scale mechanisms. Advances in Geo-Energy Research, 2024c, 13(3): 203-217.

Liang, Y., Tsuji, S., Jia, J., et al. Modeling CO_2-water-mineral wettability and mineralization for carbon geosequestration. Accounts of Chemical Research, 2017, 50(7): 1530-1540.

Liao, X., Lu, R., Xia, L., et al. Density functional theory for electrocatalysis. Energy & Environmental Materials, 2022, 5(1): 157-185.

Lin, X., Li, Z., Jiang, Z., et al. Simulation of methane occurrence in rough nanokerogen slits. Energy & Fuels, 2023, 37(20): 15476-15489.

Liu, L., Frouté, L., Kovscek, A. R., et al. Scale translation yields insights into gas adsorption under nanoconfinement. Physics of Fluids, 2024, 36(7): 072011.

Lv, P., Liu, Y., Jiang, L., et al. Experimental determination of wettability and heterogeneity effect on CO_2 distribution in porous media. Greenhouse Gases: Science and Technology, 2016, 6(3): 401-415.

Ma, X., Wang, H., Zhou, S., et al. Deep shale gas in china: Geological characteristics and development strategies. Energy Reports, 2021, 7: 1903-1914.

Mendel, N., Sîretanu, D., Sîretanu, I., et al. Interlayer cation-controlled adsorption of carbon dioxide in anhydrous montmorillonite clay. The Journal of Physical Chemistry C, 2021, 125(49): 27159-27169.

Mirchi, V., Dejam, M., Alvarado, V. Interfacial tension and contact angle measurements for hydrogen-methane mixtures/brine/oil-wet rocks at reservoir conditions. International Journal of Hydrogen Energy, 2022, 47(82): 34963-34975.

Miyazawa, K., Kobayashi, N., Watkins, M., et al. A relationship between three-dimensional surface hydration structures and force distribution measured by atomic force microscopy. Nanoscale, 2016, 8(13): 7334-7342.

Monroe, J., Barry, M., DeStefano, A., et al. Water structure and properties at hydrophilic and hydrophobic surfaces. Annual Review of Chemical and Biomolecular Engineering, 2020, 11(1): 523-557.

Mouzon, J., Bhuiyan, I. U., Hedlund, J. The structure of montmorillonite gels revealed by sequential cryo-XHR-SEM imaging. Journal of Colloid and Interface Science, 2016, 465: 58-66.

Muhammed, N. S., Haq, B., Al Shehri, D. CO_2 rich cushion gas for hydrogen storage in depleted gas reservoirs: Insight on contact angle and surface tension. International Journal of Hydrogen Energy, 2024, 50: 1281-1301.

Nabizadeh, A., Hassanzadeh, H., Sharifi, M., et al. Effects of dynamic contact angle on immiscible two-phase flow displacement in angular pores: A computational fluid dynamics approach. Journal of Molecular Liquids, 2019, 292: 111457.

Nandi, M., Uyama, H. Exceptional CO_2 adsorbing materials under different conditions. The Chemical Record, 2014,

14(6): 1134-1148.
Nasralla, R. A., Nasr-El-Din, H. A. Double-layer expansion: Is it a primary mechanism of improved oil recovery by low-salinity waterflooding? Society of Petroleum Engineers Reservoir Evaluation & Engineering, 2014, 17(1): 49-59.
Nemer, M. N., Rao, P. R., Schaefer, L. Coupled influence of wettability alteration and geometry on two-phase flow in porous media. Advances in Water Resources, 2021, 157: 104055.
Nie, H., Jin, Z., Li, P., et al. Deep shale gas in the Ordovician-Silurian Wufeng-Longmaxi formations of the Sichuan Basin, SW china: Insights from reservoir characteristics, preservation conditions and development strategies. Journal of Asian Earth Sciences, 2023, 244: 105521.
Nowrouzi, I., Manshad, A. K., Mohammadi, A. H. Effects of ions and dissolved carbon dioxide in brine on wettability alteration, contact angle and oil production in smart water and carbonated smart water injection processes in carbonate oil reservoirs. Fuel, 2019, 235: 1039-1051.
Pan, B., Gong, C., Wang, X., et al. The interfacial properties of clay-coated quartz at reservoir conditions. Fuel, 2020, 262: 116461.
Pan, S., Guo, R., Björnmalm, M., et al. Coatings super-repellent to ultralow surface tension liquids. Nature Materials, 2018, 17(11): 1040-1047.
Park, J., Han, H. S., Kim, Y. C., et al. Direct and accurate measurement of size dependent wetting behaviors for sessile water droplets. Scientific Reports, 2015, 5(1): 18150.
Parker, J. L., Claesson, P. M., Attard, P. Bubbles, cavities, and the long-ranged attraction between hydrophobic surfaces. The Journal of Physical Chemistry, 1994, 98(34): 8468-8480.
Purdue, M. J., Qiao, Z. Molecular simulation study of wet flue gas adsorption on zeolite 13X. Microporous and Mesoporous Materials, 2018, 261: 181-197.
Qin, X., Xia, Y., Qiao, J., et al. Modeling of multiphase flow in low permeability porous media: Effect of wettability and pore structure properties. Journal of Rock Mechanics and Geotechnical Engineering, 2024, 16(4): 1127-1139.
Rao, Q., Leng, Y. Molecular understanding of CO_2 and H_2O in a montmorillonite clay interlayer under CO_2 geological sequestration conditions. The Journal of Physical Chemistry C, 2016, 120(5): 2642-2654.
Raza, A., Mahmoud, M., Alafnan, S., et al. H_2, CO_2, and CH_4 adsorption potential of kerogen as a function of pressure, temperature, and maturity. International Journal of Molecular Sciences, 2022, 23(21): 12767.
Ruthven, D. M. Principles of Adsorption and Adsorption Processes. New York, USA, John Wiley & Sons, 1984.
Selem, A. M., Agenet, N., Blunt, M. J., et al. Pore-scale processes in tertiary low salinity waterflooding in a carbonate rock: Micro-dispersions, water film growth, and wettability change. Journal of Colloid and Interface Science, 2022, 628: 486-498.
Shao, Z., Tan, B., Li, T., et al. Study on oxidation and pyrolysis characteristics of lignite damaged by liquid CO_2 at low-temperature. Fuel, 2022, 323: 124371.
Sharma, A., Namsani, S., Singh, J. K. Molecular simulation of shale gas adsorption and diffusion in inorganic nanopores. Molecular Simulation, 2015, 41(5-6): 414-422.
Shen, C., Worek, W. Cosorption characteristics of solid adsorbents. International Journal of Heat and Mass Transfer, 1994, 37(14): 2123-2129.
Snoeijer, J. H., Andreotti, B. A microscopic view on contact angle selection. Physics of Fluids, 2008, 20: 057101.
Song, W., Liu, F., Li, Y., et al. Pore scale modeling of fluid transport in complex reservoirs: Multi-scale digital rock construction, flow experiments and simulation methods. Capillarity, 2024, 11(3): 81-88.
Song, P., Wang, H. High-performance polymeric materials through hydrogen-bond cross-linking. Advanced Materials, 2020, 32(18): 1901244.
Sui, H., Zhang, F., Wang, Z., et al. Effect of kerogen maturity, water content for carbon dioxide, methane, and their mixture adsorption and diffusion in kerogen: A computational investigation. Langmuir, 2020, 36(33): 9756-9769.
Sun, J., Chen, C., Zhang, Y., et al. Competitive adsorption characteristics based on partial pressure and adsorption mechanism of CO_2/CH_4 mixture in shale pores. Chemical Engineering Journal, 2022, 430: 133172.
Tesson, S., Firoozabadi, A. Methane adsorption and self-diffusion in shale kerogen and slit nanopores by molecular simulations. The Journal of Physical Chemistry C, 2018, 122(41): 23528-23542.
Tian, X., Kalbasi, R., Jahanshahi, R., et al. Competition between intermolecular forces of adhesion and cohesion in the presence of graphene nanoparticles: Investigation of graphene nanosheets/ethylene glycol surface tension. Journal of Molecular Liquids, 2020, 311: 113329.
Van Honschoten, J. W., Brunets, N., Tas, N. R. Capillarity at the nanoscale. Chemical Society Reviews, 2010, 39(3): 1096-1114.
Wang, H., Cai, J., Su, Y., et al. Pore-scale study on shale oil-CO_2-water miscibility, competitive adsorption, and multiphase flow behaviors. Langmuir, 2023, 39(34): 12226-12234.
Wang, F., Chang, S. Molecular dynamics investigation of shale oil occurrence and adsorption in nanopores: Unveiling wettability and influencing factors. Chemical Engineering Journal, 2024, 481: 148380.
Wang, S., Han, S., Sang, S., et al. Adsorption characteristics and storage models of subcritical/supercritical CO_2 in coal seams. Natural Gas Industry Journal, 2024, 44(6): 152-168. (in Chinese)
Wang, Q., Xu, S., Xing, X., et al. Progress in fabrication and applications of micro/nanostructured superhydrophobic surfaces. Surface Innovations, 2021, 10(2): 89-110.
Wang, X., Zhang, Q. Role of surface roughness in the wettability, surface energy and flotation kinetics of calcite. Powder Technology, 2020, 371: 55-63.
Wenzel, R. N. Resistance of solid surfaces to wetting by water. Industrial & Engineering Chemistry, 1936, 28(8): 988-994.
Widom, B. Capillarity and wetting phenomena: Drops, bub-

bles, pearls, waves. Physics Today, 2004, 57(12): 66-67.
Wróblewski, P., Kachel, S. The concept of the contact angle in the process of oil film formation in internal combustion piston engines. Scientific Reports, 2023, 13(1): 20715.
Wu, J. Understanding the electric double-layer structure, capacitance, and charging dynamics. Chemical Reviews, 2022, 122(12): 10821-10859.
Xu, W., Fayaz-Torshizi, M., Müller, E. A. Effect of surface roughness and morphology on the adsorption and transport of CH_4/CO_2 mixtures in nanoporous carbons. Journal of CO_2 Utilization, 2024, 79: 102649.
Xu, R., Li, R., Ma, J., et al. Effect of mineral dissolution/precipitation and CO_2 exsolution on CO_2 transport in geological carbon storage. Accounts of Chemical Research, 2017, 50(9): 2056-2066.
Xu, C., Xue, H., Li, B., et al. Microscopic adsorption mechanism difference in the mineral pore of shale gas reservoir. Special Oil & Gas Reservoirs, 2020, 27(4): 80-84.
Xu, S., Zhou, S., Zhou, J., et al. Multiscale pore structure evolution of Longmaxi shale induced by acid treatment. Society of Petroleum Engineers Journal, 2023, 28(02): 831-844.
Yadav, A., Taha, A., Abdulsayed, Y. A., et al. A density functional theory (DFT) study on adsorption of a biological active ethionamide over the surface of a fe-decorated porphyrin system. Chemical Review and Letters, 2023, 6(2): 128-138.
Yan, Z., Wang, F., Liu, Y., et al. Dynamic wetting of a CO_2-H_2O-montmorillonite system using molecular dynamics. Fuel, 2024, 377: 132787.
Yang, Y., Liu, F., Yao, J., et al. Multi-scale reconstruction of porous media from low-resolution core images using conditional generative adversarial networks. Journal of Natural Gas Science and Engineering, 2022, 99: 104411.
Yang, Y., Narayanan Nair, A. K., Sun, S. Adsorption and diffusion of carbon dioxide, methane, and their mixture in carbon nanotubes in the presence of water. The Journal of Physical Chemistry C, 2020, 124(30): 16478-16487.
Yang, Y., Song, H., Imani, G., et al. Adsorption behavior of shale oil and water in the kerogen-kaolinite pore by molecular simulations. Journal of Molecular Liquids, 2024, 393: 123549.
Yang, X., Zhao, H., Qu, Z., et al. The effect of oxygen-containing functional groups on formaldehyde adsorption in solution on carbon surface: A density functional theory study. Journal of Environmental Chemical Engineering, 2021, 9(5): 105987.
Yeon, J., Chowdhury, S. C., Gillespie Jr, J. W. Hydroxylation and water-surface interaction for S-glass and silica glass using ReaxFF based molecular dynamics simulations. Applied Surface Science, 2023, 608: 155078.
Yi, H., Jia, F., Zhao, Y., et al. Surface wettability of montmorillonite (0 0 1) surface as affected by surface charge and exchangeable cations: A molecular dynamic study. Applied Surface Science, 2018, 459: 148-154.
Young, T. III. An essay on the cohesion of fluids. Philosophical Transactions of the Royal Society of London, 1805, (95): 65-87.
Youngblood, J. P., McCarthy, T. J. Ultrahydrophobic polymer surfaces prepared by simultaneous ablation of polypropylene and sputtering of poly (tetrafluoroethylene) using radio frequency plasma. Macromolecules, 1999, 32(20): 6800-6806.
Yuan, J., Luo, D., Feng, L. A review of the technical and economic evaluation techniques for shale gas development. Applied Energy, 2015, 148: 49-65.
Zhang, W., Feng, Q., Jin, Z., et al. Molecular simulation study of oil-water two-phase fluid transport in shale inorganic nanopores. Chemical Engineering Science, 2021, 245: 116948.
Zhang, J., Guo, B., Amponsah, V. N. B. A more rigorous mathematical model for capillary imbibition of CO_2 in shale gas formations. Capillarity, 2025a, 14(3): 63-71.
Zhang, X., Guo, P., Gao, X., et al. Crack and failure behaviors of sandstone subjected to dynamic loads visualized by micro-computed tomography. Journal of Rock Mechanics and Geotechnical Engineering, 2025b, 17(3): 1459-1473.
Zhang, Y., Shi, L., Lan, L., et al. Interaction pattern of dense sandstone with CO_2, and water. Science Technology and Engineering, 2025c, 25(3): 1028-1038. (in Chinese)
Zhang, S., Wang, T., Gao, Z., et al. Wettability controlling effects on the fluid occurrence and flow in shale gas reservoirs: Present problems and new sights. Capillarity, 2023, 9(2): 25-31.
Zhao, J. Fundamental and application research of CO_2 and H_2O competitive adsorption on carbon capture. Tianjin, Tianjin University, 2022. (in Chinese)
Zhao, J., Deng, S., Zhao, L., et al. Synergistic and competitive effect of H_2O on CO_2 adsorption capture: Mechanism explanations based on molecular dynamic simulation. Journal of CO_2 Utilization, 2021, 52: 101662.
Zheng, Y., Huang, R., Yu, Y., et al. Synergistic effects of hydrophilic function group and micropores on water evaporation in a novel carbon hydrogels for efficient solar steam generation. Water Research, 2024, 257: 121707.
Zhou, J., Jin, Z., Luo, K. The role of brine in gas adsorption and dissolution in kerogen nanopores for enhanced gas recovery and CO_2 sequestration. Chemical Engineering Journal, 2020, 399: 125704.